Predicted band structures of III-V semiconductors in the wurtzite phase

A. De and Craig E. Pryor
Department of Physics and Astronomy and Optical Science and Technology Center, University of Iowa, Iowa City, Iowa 52242, USA
(Received 6 August 2009; revised manuscript received 19 February 2010; published 20 April 2010; corrected 5 May 2010)

While non-nitride III-V semiconductors typically have a zinc-blende structure, they may also form wurtzite crystals under pressure or when grown as nanowhiskers. This makes electronic structure calculation difficult since the band structures of wurtzite III-V semiconductors are poorly characterized. We have calculated the electronic band structure for nine III-V semiconductors in the wurtzite phase using transferable empirical pseudopotentials including spin-orbit coupling. We find that all the materials have direct gaps. Our results differ significantly from earlier *ab initio* calculations, and where experimental results are available (InP, InAs, and GaAs) our calculated band gaps are in good agreement. We tabulate energies, effective masses, and linear and cubic Dresselhaus zero-field spin-splitting coefficients for the zone-center states. The large zero-field spin-splitting coefficients we find may facilitate the development of spin-based devices.

DOI: 10.1103/PhysRevB.81.155210 PACS number(s): 61.82.Fk, 71.20.−b, 71.15.Dx, 61.72.uj

I. INTRODUCTION

Semiconductor nanowhiskers (NWs) have attracted a tremendous amount of interest in recent years.[1–8] Much of it is due to their potential application in areas such as photovoltaic cells,[9–11] nanoelectromechanical resonator arrays,[12] microwave and terahertz detection,[13,14] single photon detection,[15–17] field-effect[18,19] and single-electron transistors,[20] and various other electronic and optoelectronic devices.[21–25] NWs are also interesting because one-dimensional systems can be made using material combinations for which large lattice mismatches prohibit quantum well structures, allowing greater freedom in material combinations for device engineering.

In contrast to bulk non-nitride III-V materials which are usually zinc-blende (ZB), NWs predominantly crystallize in the wurtzite (WZ) phase.[26–28] Several different theoretical explanations for this behavior have been proposed. Recent calculations suggest that the WZ phase is energetically favorable for small NW radii,[29,30] although this does not account for all NW radii for which the WZ phase is experimentally observed. Calculations based on an empirical nucleation model indicate that WZ formation is favored for certain ranges of the interface energies.[31] *Ab initio* calculations indicate that the WZ phase is favored due to the accumulation of electrons at the interstitial site containing the Au catalyst,[32] while other calculations show that the polytype is determined by growth kinetics.[33] It should be noted that these different mechanisms are not necessarily mutually exclusive.

A theoretical understanding of the electronic and optical properties of semiconductor nanostructures is based on a knowledge of the electronic properties of bulk materials. However, little is known about the electronic band structure of III-V semiconductors in the WZ phase since most do not naturally occur as bulk crystals. Moreover, the NWs often contain sections of ZB material forming heterostructures out of the differing band structures of the two polytypes.[2,34–36] Band structures of WZ III-V semiconductors have been calculated using density-functional theory (DFT) in the local-density approximation (LDA).[37,38] Since the LDA underestimates band gaps the WZ band structure cannot be directly determined, and instead calculations of WZ and ZB are typically compared to obtain the differences between the two polytypes. The band structures of GaAs and InAs in the WZ phase have also been calculated using the GW method[39] giving somewhat different results than those from the LDA. In addition to the inherent errors in *ab initio* band gaps, all of the above calculations neglected the spin-orbit coupling, which is known to significantly alter the valence-band structure of semiconductors.

In this paper we present calculations of the bulk electronic band structures of the nine non-nitride III-V semiconductors in the WZ phase using empirical pseudopotentials including spin-orbit coupling. These calculations are based on transferable model pseudopotentials assuming ideal WZ structure. The spherically symmetric ionic model potentials are first obtained by fitting the calculated bulk ZB energies to experimental energies at high symmetry points. The band structure of the WZ polytype is then obtained by transferring the model pseudopotentials to the WZ pseudopotential Hamiltonian using the appropriate crystal structure factors.

This method has been proven to be very successful in obtaining the bulk band structures of semiconductor polytypes.[40–48] The anion and cation pseudopotentials are specific to each material and are only transferred between polytypes. Therefore, the model potentials should be transferable between ZB and WZ polytypes due to the similarities in their crystal structures. In both structures all of the nearest neighbors and nine out of the 12 second-nearest neighbors are at identical crystallographic locations[49] while the second-nearest neighbors are equidistant.

This paper is organized as follows. In Sec. II we outline the similarities and differences between ZB and WZ crystal structures as well as the direct correspondence between high symmetry k points in the two polytypes. In Sec. III we describe the transferable pseudopotential method. In Sec. IV we present the calculated band structures, their respective density of states (DOS), and effective masses. Finally, we summarize the results in Sec. V.

 ©2010 The American Physical Society

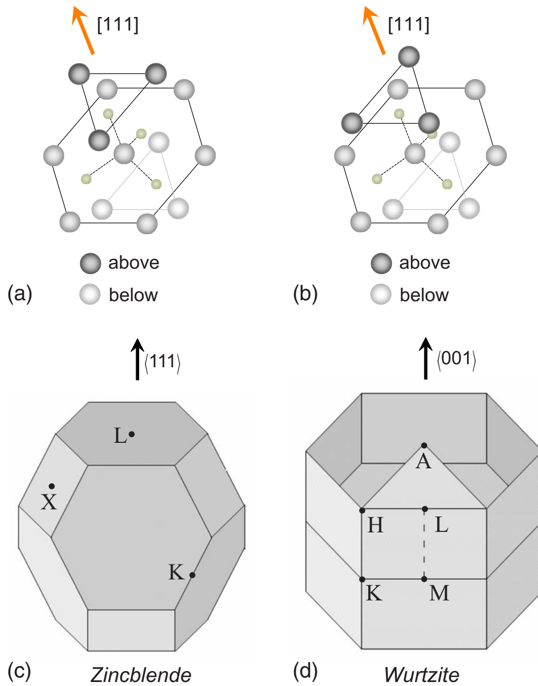

FIG. 1. (Color online) (a) Staggered configurations of atom-1 as viewed along [111] for ZB. (b) Eclipsed configuration of atom-1 as viewed along [111] for WZ. Note that nine out of the 12 second-nearest neighbors are in the same position. The other three are rotated by $\pi/3$. (c) Brillouin zone for ZB. (d) Brillouin zone for WZ. Γ is at the center of the Brillouin zones.

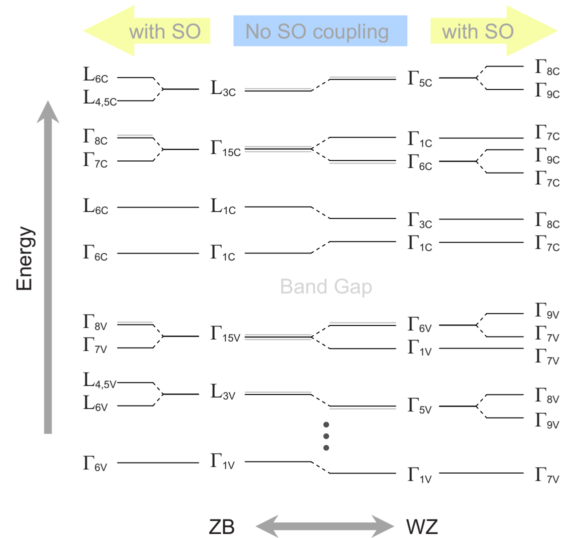

FIG. 2. (Color online) Schematic showing the correspondence between energy levels at the L and Γ points in ZB and the Γ point in WZ with and without spin-orbit coupling (Ref. 37). The dashed lines show the correspondence between the states. Additional degenerate levels are shown in gray.

II. WURTZITE VERSUS ZINCBLENDE

A. Crystal structure

The ZB crystal is formed by two interpenetrating face-centered-cubic (fcc) Bravais lattices (each of a different atomic species), whereas the WZ structure is constructed from two interpenetrating hexagonal-close-packed (hcp) lattices. The differences between the two structures are best understood by viewing along the [111] direction [Figs. 1(a) and 1(b)], along which both look like stacked hexagonal layers. The atoms are identical within each layer, and the layers alternate between the anion and the cation. For the ideal WZ crystal the lattice constant is given by $a_{WZ}=a_{ZB}/\sqrt{2}$ and the lattice constant along the c axis (axis perpendicular to the hexagon) is related to the in-plane lattice constant by $c=\sqrt{8/3}\ a_{WZ}$. Since the WZ crystal is tetrahedral, the nearest neighbors are the same in the two polytypes. In addition, we see from Fig. 1 that nine of the 12 nearest neighbors in WZ are the same as in ZB. These structural similarities suggest that the local electronic environment will be the same in the two crystals, and therefore the crystal potentials will be nearly identical in WZ and ZB.

In WZ the type-1 atoms are located at (0,0,0) and $\frac{2}{3}\mathbf{a}_1+\frac{1}{3}\mathbf{a}_2+\frac{1}{2}\mathbf{a}_3$, while the type-2 atoms are located at $u\mathbf{a}_3$ and $\frac{2}{3}\mathbf{a}_1+\frac{1}{3}\mathbf{a}_2+(\frac{1}{2}+u)\mathbf{a}_3$, where the primitive lattice vectors are $\mathbf{a}_1=(1,\sqrt{3},0)a_{WZ}/2$, $\mathbf{a}_2=(1,-\sqrt{3},0)a_{WZ}/2$, and $\mathbf{a}_3=(0,0,c)$.

Throughout this paper we assume an ideal WZ crystal with $u=3/8$. The most studied WZ semiconductors are nitride III-Vs, which have values of u ranging from 0.3783 (GaN) to 0.3902 (AlN).[50] Relatively little is known about the structure of non-nitride WZ III-Vs. Measurements of bulk samples of metastable WZ GaAs give $u=0.3693$,[51] while InAs nanowires have an ideal WZ structure with $u=0.37502$.[39] The paucity of data on non-nitride III-Vs and the fact that the one structural measurement in an actual nanowire indicates the ideal structure support the assumption of an ideal WZ crystal until better data become available.

In lieu of experimental data, an alternative to using the ideal WZ structure would be to calculate the WZ lattice constants using DFT. However, for materials that have been measured, the ideal structure is in fact more accurate than that obtained from DFT. For example, the calculated lattice constants of WZ GaN differ from experiment by −1.4% to +1.0% for a, and −1.1% to +1.4% for c,[52] and other calculations differ by 3%.[38] In contrast, the ideal GaN structure differs from experiment by +0.2% for a and −0.2% for c. As a test of the overall accuracy of our method for determining band structures, we calculated the band structure of GaN using the ideal lattice constants obtaining $E_g=3.477$ eV which is in good agreement with the experimental value $E_g=3.503$ eV.[53]

B. Band structure

Due to the similarities of the two crystals, many of the high symmetry points in the Brillouin zones of ZB and WZ are related to each other and an understanding of their correspondences is useful for understanding trends in the band structures of the two polytypes. Figure 2 shows the relationships among the zone-center states in WZ and the corresponding L and Γ points in ZB, both with and without spin-orbit coupling. One of the most important features is that in the empty lattice approximation the L point in ZB is zone-folded to the Γ point in WZ. As a result, in the absence of

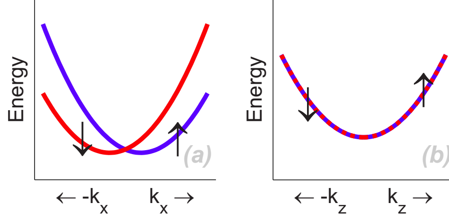

FIG. 3. (Color online) (a) Zero-field Dresselhaus spin splitting in WZ along k_x for a Γ_7 conduction band. (b) The zero-field spin splitting is not seen along the k_z direction.

spin-orbit coupling, the Γ_1, L_1, and L_3 states in ZB correspond to Γ_1, Γ_3, and Γ_5, respectively, in WZ (Fig. 2). Because of this folding over of the L valley, indirect gap ZB materials with an L valley conduction-band minimum would be expected to have a direct gap in the ZB phase unless the energy of the state was significantly shifted by the crystal potential.

The states at the top of the valence band in WZ also have some important differences with their ZB counterparts. In the absence of spin-orbit coupling, the hexagonal crystal field of WZ splits the p-like Γ_{15} state of ZB into a fourfold degenerate Γ_6 and a doubly degenerate Γ_1. In terms of the p orbitals, these states are $p_z \rightarrow \Gamma_1$ are $p_x, p_y \rightarrow \Gamma_6$. With the inclusion of spin-orbit coupling, Γ_{6v} splits into the Γ_{9v} heavy hole and the Γ_{7v} light hole. Therefore, all zone-center states in WZ belong to either Γ_7, Γ_8, or Γ_9. There are similar correspondences between the high symmetry directions of the two crystals. The symmetry line $\Lambda(\Gamma \rightarrow L)$ in ZB corresponds to the $\Delta(\Gamma \rightarrow A)$ line in WZ.[49]

C. Spin splitting

For certain individual states in crystals lacking inversion symmetry, spin-orbit coupling causes a splitting of spin-up and spin-down states which leads to $E_\uparrow(-\mathbf{k}) \neq E_\uparrow(\mathbf{k})$ (see Fig. 3). The states at $\mathbf{k}=0$ are still twofold degenerate resulting in a nonvanishing $\nabla_k E(\mathbf{k})$ at the origin for certain crystallographic directions. In the case of WZ, the states remain spin-degenerate for k along the c axis because at any point along the k_z direction $(\Gamma \rightarrow A)$, the crystallographic point group is C_{6v}.[54] As all the irreducible representations (IR) compatible with spin $(\Gamma_{7,8,9})$ in this group are doubly degenerate,[55] there is no spin splitting along k_z.

In WZ, the spin-splitting effects near the zone center can be described with an effective one band Hamiltonian[56–58]

$$H(\mathbf{k}) \propto \frac{k_x^2 + k_y^2}{2m_\perp} + \frac{k_z^2}{2m_\parallel} + \sum_{n=0}^{\infty} \alpha_n [\sigma_x k_y + \sigma_y k_x]^{(2n+1)}, \quad (1)$$

where α_n are constants. This effective Hamiltonian is invariant with respect to C_{6v} for all odd powers of k. The coefficients of the linear and cubic Dresselhaus spin-splitting terms can be obtained by expanding Eq. (1) up to $n=1$. Near the crossing, the difference in energies between the spin-split bands in Fig. 3(a) has the form[58]

$$|E_{i,\uparrow}(k) - E_{i,\downarrow}(k)| = 2\zeta_1^i k + \zeta_3^i k^3, \quad (2)$$

where ζ_1^i and ζ_3^i are the linear and cubic Dresselhaus spin-splitting coefficients, respectively, for band i. These coefficients characterize the spin splitting and may be determined from the computed band structure by fitting a function of the above form. While the existence of a spin splitting in a particular direction is determined by symmetry considerations,[54] the magnitude can vary considerably. Although both ZB and WZ crystals lack inversion symmetry, spin-splitting effects are much more prominent in WZ due to its lower crystal symmetry,[58–69] which can be of particular use in spintronic devices.

III. METHOD

A. Pseudopotentials

Our band structures are computed using the empirical pseudopotential method of Cohen and Chelikowsky[48] with a model potential applicable to both ZB and WZ structures. Pseudopotentials exploit the fact that the electronic wave function may be separated into the sum of a rapidly oscillating part near the atomic cores and a slowly varying piece. The pseudopotential approach relies on the assumption that the core electrons are frozen and that the valence electrons move in a weak single-electron potential making the true atomic wave function orthogonal to the core states. The pseudowave equation is then

$$\left(\frac{p^2}{2m} + V_{pp}\right)|\phi\rangle = E|\phi\rangle, \quad (3)$$

where $|\phi\rangle$ is the smoothly varying pseudowave function, and V_{pp} is the pseudopotential which includes a repulsive core to partially cancel the deep potential near the atomic core.[70] By taking V_{pp} to be a local pseudopotential which is a function only of position, it may be expanded in terms of reciprocal lattice vectors, $\mathbf{G}$, as

$$V_{pp}(\mathbf{r}) = \sum_{\mathbf{G},\alpha} V_\alpha^{FF}(\mathbf{G}) S_\alpha(\mathbf{G}) e^{i\mathbf{G}\cdot\mathbf{r}}, \quad (4)$$

$$S_\alpha(\mathbf{G}) = \frac{1}{N_\alpha} \sum_{i=1}^{N_\alpha} e^{-i\mathbf{G}\cdot\boldsymbol{\tau}_{\alpha,i}}, \quad (5)$$

where α labels the atom type, $V_\alpha^{FF}(\mathbf{G})$ is the form factor, $S_\alpha(\mathbf{G})$ is the structure factor, N_α is the number of atoms per unit cell of type α, and $\boldsymbol{\tau}_{\alpha,i}$ is the position of atom number i of type α.

For binary compounds it is convenient to separate the pseudopotential into symmetric (S) and antisymmetric (A) parts as

$$\langle \mathbf{G}'|V_{pp}|\mathbf{G}\rangle = V_S(\mathbf{G}'-\mathbf{G}) S_S(\mathbf{G}'-\mathbf{G}) + iV_A(\mathbf{G}'-\mathbf{G}) S_A(\mathbf{G}'-\mathbf{G}). \quad (6)$$

The symmetric and antisymmetric structure factors are given by

$$S_S(\mathbf{G}) = \frac{1}{N} \sum_j \exp(-i\mathbf{G}\cdot\boldsymbol{\tau}_j), \quad (7)$$

TABLE I. Fitting parameters for symmetric and antisymmetric form factors, where the form factors are in units of Ry. μ_1 and μ_2 are the fitting parameters for the spin-orbit coupling. The values in the table have been rounded to save space.

Material	x_1	x_2	x_3	x_4	x_1'	x_2'	x_3'	x_4'	μ_1	μ_2
AlP	0.083	−0.579	0.031	−2.586	−0.11	0.9	−0.061	−1.178	0.012	0
AlAs	0.062	−0.459	0.027	−2.629	−0.041	1.003	−0.056	−1.693	5.28×10^{-3}	5×10^{-5}
AlSb	0.06	−0.412	0.032	−2.548	−0.09	0.17	−0.051	−2.098	7.26×10^{-3}	2.96×10^{-4}
GaP	0.085	−0.457	0.04	−2.566	−0.351	5.165	−0.205	0.339	0.385	-2.3×10^{-3}
GaAs	0.058	−0.467	0.023	−2.583	−0.063	1.091	−0.074	−1.298	0.052	8.3×10^{-6}
GaSb	0.042	−0.343	0.022	−2.584	−0.009	0.618	−0.043	−2.233	0.056	2.78×10^{-5}
InP	0.049	−0.385	0.027	−2.602	0	0.847	−0.059	−1.654	0.243	-1.09×10^{-3}
InAs	0.036	−0.298	0.033	−2.615	−0.011	1.359	−0.121	−1.124	0.082	2.603×10^{-5}
InSb	0.022	−0.174	0.023	−2.42	−0.012	1.158	−0.082	−1.363	0.085	5.7×10^{-5}

$$S_A(\mathbf{G}) = \frac{-i}{N}\sum_j P_j \exp(-i\mathbf{G}\cdot\boldsymbol{\tau}_j), \quad (8)$$

where N is the number of atoms per unit cell and $P_j=+1$ for one type of atom and −1 for the other type. The symmetric and antisymmetric form factors, $V_A(\mathbf{G})$ and $V_S(\mathbf{G})$, are obtained from the sum and difference of the spherically symmetric anion and cation potentials.

There are several approaches to calculating V_{FF}.[48,71] In the empirical pseudopotential approach used here, $V_S(\mathbf{G})$ and $V_A(\mathbf{G})$ are adjusted to fit the calculated energy spectrum to experimentally determined energies at band extrema. Model potentials that yield an accurate band structure of a known polytype should reliably predict the band structure for the unknown polytype if the two crystal structures are similar. To compute the WZ band structure using pseudopotentials obtained from ZB requires $V_S(\mathbf{G})$ and $V_A(\mathbf{G})$ to be continuous functions that can be evaluated at any value of $\mathbf{G}$. A wide variety of model potentials have been used[44,71–74] and we use potentials of the form

$$V_S(\mathbf{G}) = \frac{x_1 G - x_2}{\exp(x_3 G^2 + x_4) + 1}, \quad (9)$$

$$V_A(\mathbf{G}) = (x_1' G^2 + x_2')\exp(x_3' G^2 + x_4'), \quad (10)$$

where $G=|\mathbf{G}|$, and the parameters x_j and x_j' are obtained for each material by fitting to the ZB band structure.

B. Spin-orbit interactions

We include the spin-orbit coupling, given by

$$H_{so} = \frac{\hbar^2}{4m^2c^2}[\nabla V(\mathbf{r}) \times \mathbf{p}]\cdot\boldsymbol{\sigma}, \quad (11)$$

using the method of Weisz.[75] Equation (11) cannot be used directly since spin-orbit coupling involves the core states which are omitted from the pseudowave equation as a result of orthogonalization. Instead, by returning to the original Schrödinger equation we may expand in terms of the core states $|\phi_c\rangle$ to obtain[75,76]

$$\langle\phi'|V_{so}|\phi\rangle \approx \sum_{c,c'} \langle\phi'|\phi_{c'}\rangle\langle\phi_{c'}|H_{so}|\phi_c\rangle\langle\phi_c|\phi\rangle. \quad (12)$$

In this way the matrix elements of H_{so} for core states may be parametrized and then fit to experiment in the same way as the pseudopotential form factors. By expanding $|\phi\rangle$ in Bloch

TABLE II. Ratios of calculated/targeted band transition energies at various high symmetry points for nine III-V zinc-blende semiconductors. All transition energies are referenced to the top of valence band, (E_{8v}^{Γ}). The spin-orbit energies are $\Delta_{so}=E_{8v}^{\Gamma}-E_{7v}^{\Gamma}$ and $\Delta_{so}'=E_{8c}^{\Gamma}-E_{7c}^{\Gamma}$. In addition, the effective for the conduction band (m_c), split-off bands (m_{so}), and heavy and light holes are compared to those from Ref. 79. The heavy and light hole masses are expressed in terms of Luttinger parameters γ_1, γ_2 and γ_3 [see Eq. (25)]. Note that the effective masses were not set as targets for fitting the form factors.

Material	E_{6c}^{Γ}	Δ_{so}	E_{6c}^{L}	E_{6c}^{X}	E_{7c}^{Γ}	E_{8c}^{Γ}	Δ_{so}'	E_{6v}^{Γ}	m_c	m_{so}	γ_1	γ_2	γ_3
AlP	1.00	1.00	1.00	1.00				1.03	0.72	1.06	0.92	0.99	0.95
AlAs	1.00	1.00	1.01	1.00	1.01	1.01	1.00	0.99	0.99	1.07	0.95	0.84	0.96
AlSb	1.00	1.00	1.00	1.00	1.00	1.00	1.00	0.97	1.04	1.30	0.67	0.66	0.70
GaP	1.00	1.00	1.00	1.00	1.00	1.00	1.00	0.97	1.00	1.02	0.96	1.66	1.20
GaAs	1.00	1.00	1.00	1.00	1.00	1.00	1.00	0.95	1.16	1.19	0.81	0.90	0.83
GaSb	1.00	1.00	1.01	1.00	1.00	1.00	1.00	0.94	1.47	1.56	0.63	0.61	0.62
InP	1.00	1.00	1.00	1.00	1.00	1.00	1.00	1.02	1.08	1.03	0.96	0.98	1.00
InAs	1.00	1.00	1.00	1.01	1.00	1.00	1.00	0.95	1.36	1.05	0.61	0.60	0.62
InSb	1.00	1.00	1.01	1.00	1.00	1.00	1.00	0.84	1.85	1.73	0.55	0.54	0.56

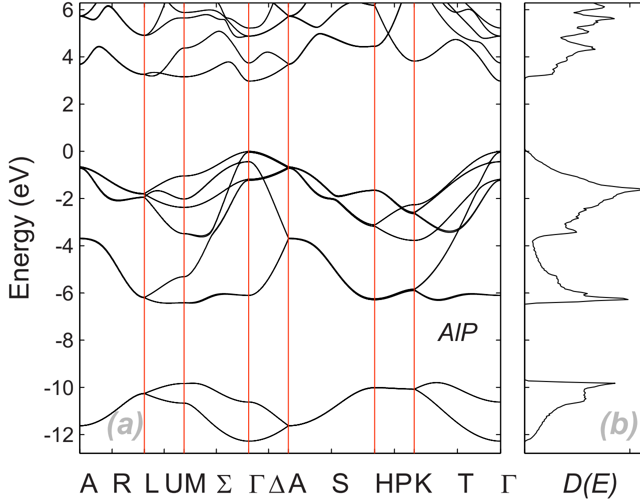

FIG. 4. (Color online) (a) Calculated band structure for AlP in wurtzite phase. (b) Calculated DOS.

functions, and expressing the core states in terms of its constituent atomic radial wave functions and respective spherical harmonics, Eq. (12) can be recast as[75]

$$\langle \mathbf{K}',s'|V_{so}|\mathbf{K},s\rangle = (\mathbf{K}'\times\mathbf{K})\cdot\langle s'|\boldsymbol{\sigma}|s\rangle \times\sum_l \lambda_l P_l'(\cos\theta_{\mathbf{K}'\cdot\mathbf{K}})S(\mathbf{K}'-\mathbf{K}), \tag{13}$$

where P_l' is the derivative of the Legendre polynomial, $\boldsymbol{\sigma}$'s are the Pauli matrices, $\mathbf{K}=\mathbf{G}+\mathbf{k}$, and θ is the angle between $\mathbf{K}$ and $\mathbf{K}'$. The coefficient λ_l is given in terms of the core wave functions by

$$\lambda_l = \mu_l \beta_{nl}(\mathbf{K}')\beta_{nl}(\mathbf{K}), \tag{14}$$

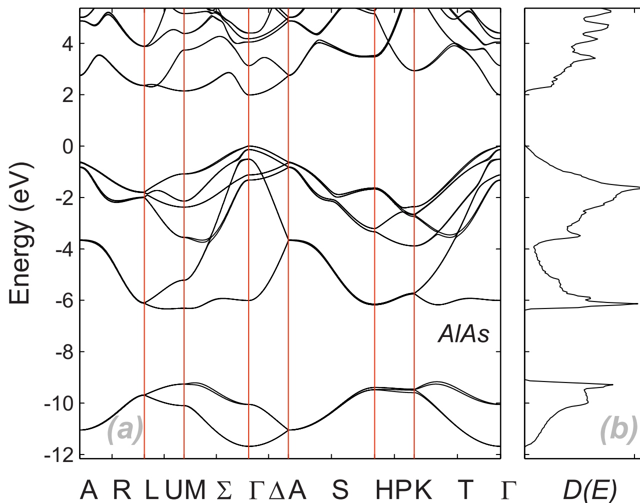

FIG. 5. (Color online) (a) Calculated band structure for AlAs in wurtzite phase. (b) Calculated DOS.

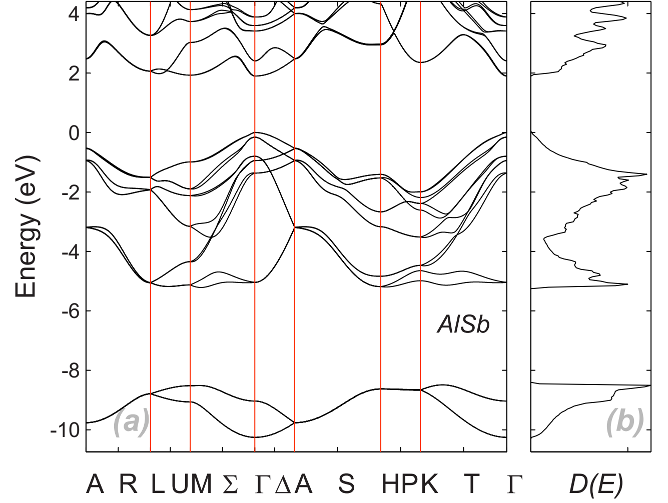

FIG. 6. (Color online) (a) Calculated band structure for AlSb in wurtzite phase. (b) Calculated DOS.

$$\beta_{nl}(K) = C\int_0^\infty i^l\sqrt{4\pi(2l+1)}\,j_{nl}(Kr)R_{nl}(r)r^2dr, \tag{15}$$

where C is a normalization constant such that $\beta_{nl}(K)/K$ approaches unity in the limit K goes to zero and n is the principal quantum number for the core state being considered. For III-V semiconductors, it is not required to expand Eq. (13) beyond $l=2$ since they do not have core shells filled beyond d orbitals. Expanding Eq. (13) up to $l=2$, the matrix elements for the spin-orbit coupling in a binary compound are

$$\langle \mathbf{K}',s'|V_{so}|\mathbf{K},s\rangle = -i(\hat{\mathbf{K}}'\times\hat{\mathbf{K}})\cdot\langle s'|\boldsymbol{\sigma}|s\rangle \times[(\lambda_p^S+\lambda_d^S\hat{\mathbf{K}}'\cdot\hat{\mathbf{K}})S_S(\mathbf{G}'-\mathbf{G}) + (\lambda_p^A+\lambda_d^A\hat{\mathbf{K}}'\cdot\hat{\mathbf{K}})S_A(\mathbf{G}'-\mathbf{G})], \tag{16}$$

$$\lambda_l^S = (\lambda_l^{(1)}+\lambda_l^{(2)})/2, \tag{17}$$

$$\lambda_l^A = (\lambda_l^{(1)}-\lambda_l^{(2)})/2, \tag{18}$$

$$\lambda_l^{(1)} = \mu_l\beta_{nl}^{(1)}(\mathbf{K}_i)\beta_{nl}^{(1)}(\mathbf{K}_j), \tag{19}$$

$$\lambda_l^{(2)} = \gamma_l\mu_l\beta_{nl}^{(2)}(\mathbf{K}_i)\beta_{nl}^{(2)}(\mathbf{K}_j), \tag{20}$$

where the superscript (1),(2) specifies which atom, the coefficient μ_l is an empirically adjusted parameter, and γ_l is the ratio of the anion to cation spin-orbit splitting energies for a given core state.[77] The overlap integral, β_{nl}, is constructed from the atomic core wave functions using Eq. (15). The radial part of the core wave function, R_{nl}, is an approximate Hartree-Fock solution taken from Herman-Skillman tables.[78] For Ga, In, As, and Sb, terms up to $l=2$ in Eq. (16) are included while Al and P only go up to $l=1$ since they do not have valence d shells. In our calculations only contributions from the outermost p and d shells are considered for the spin-orbit interactions. For the p states $n=5$ for In and Sb, $n=4$ for Ga and As, and $n=3$ for Al and P. For the d states

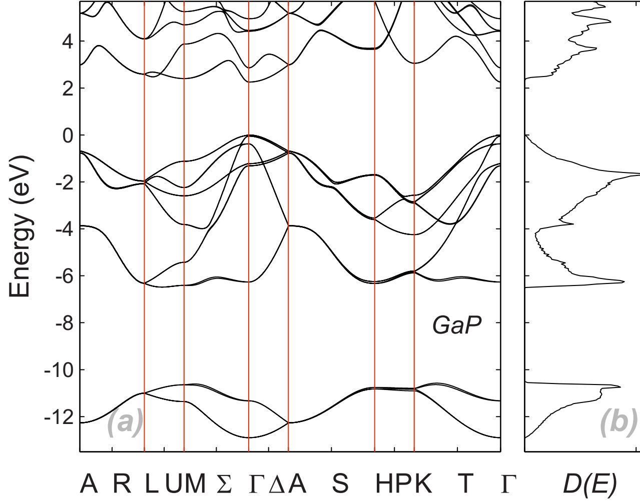

FIG. 7. (Color online) (a) Calculated band structure for GaP in wurtzite phase. (b) Calculated DOS.

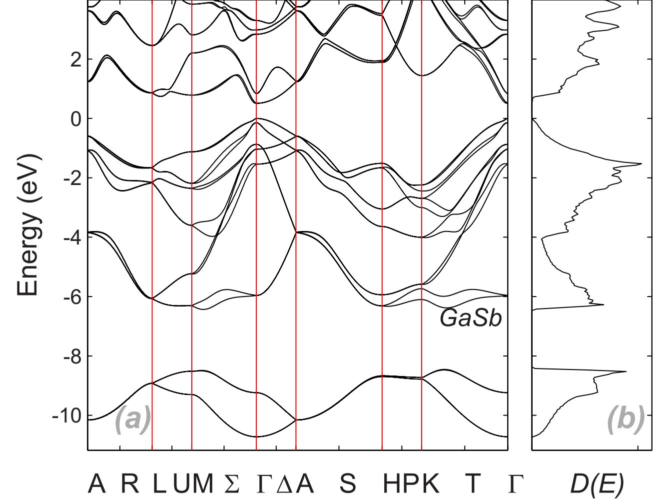

FIG. 9. (Color online) (a) Calculated band structure for GaSb in wurtzite phase. (b) Calculated DOS.

$n=4$ for In and Sb, and $n=3$ for Ga and As. With the inclusion of Eq. (16) the total pseudopotential Hamiltonian becomes

$$H = \frac{-\hbar^2 \mathbf{K}^2}{2m} + V_{pp} + V_{so}. \quad (21)$$

C. Fitting

The pseudopotential parameters x_i, x_i', and μ_l in Eqs. (9), (10), and (20) were determined by fitting the band structure obtained from the Hamiltonian of Eq. (21) to experimental energies of the band extrema of ZB materials. The Hamiltonian was evaluated in a plane-wave basis with a cutoff of $|\mathbf{G}| \leq 32\pi/a$, and for each value of $\mathbf{k}$ the Hamiltonian was diagonalized to give energies to be fit to the experimental target values. The fitting was accomplished by minimizing the error function

$$F = \sum_i W_i \frac{[E_i(\text{calculated}) - E_i(\text{target})]^2}{E_i^2(\text{target})}, \quad (22)$$

where the sum over i ranges over the targeted energies E_i, and W_i are weighting factors adjusted to speed convergence. Seven energies were used as fitting parameters (all with respect to $E_{8v}^{\Gamma}=0$): E_{6c}^{Γ}, E_{7v}^{Γ}, E_{6c}^{X}, E_{6c}^{L}, E_{v6}^{Γ}, E_{c7}^{Γ}, E_{c8}^{Γ}. The targeted values of E_{6c}^{Γ}, E_{6c}^{X}, E_{6c}^{L}, and E_{7v}^{Γ} were taken from Ref. 79 while the higher transition energies were taken from Ref. 53. In addition, constraints were imposed to ensure the correct band ordering of valence states by forcing the third and fourth (spin-degenerate) valence-band states to have Γ_7 symmetry. F was minimized with respect to x_i, x_i', and μ_i using Powell's method, with the local pseudopotential form factors from Ref. 80 used as an initial starting point. Slightly different initial values were used as a check that the solution did not converge to a spurious local minimum since Powell's method finds the local minimum. In those cases where the

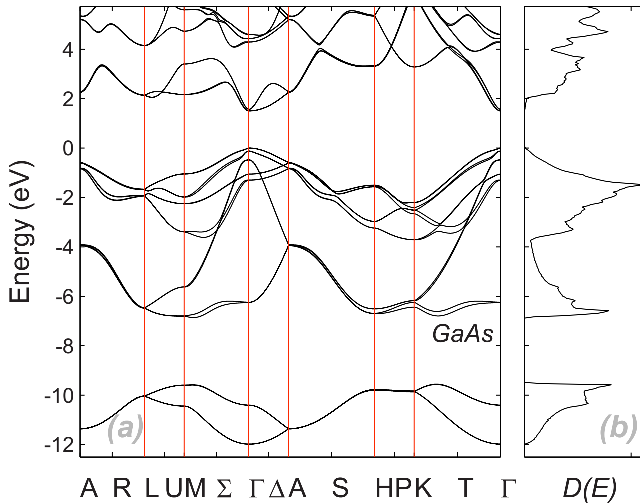

FIG. 8. (Color online) (a) Calculated band structure for GaAs in wurtzite phase. (b) Calculated DOS.

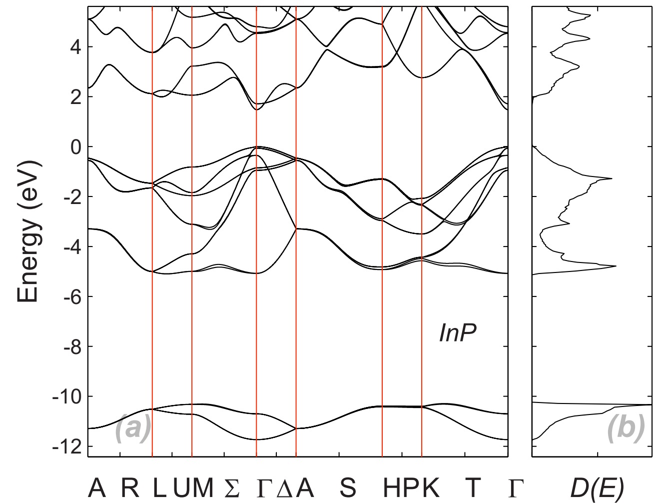

FIG. 10. (Color online) (a) Calculated band structure for InP in wurtzite phase. (b) Calculated DOS.

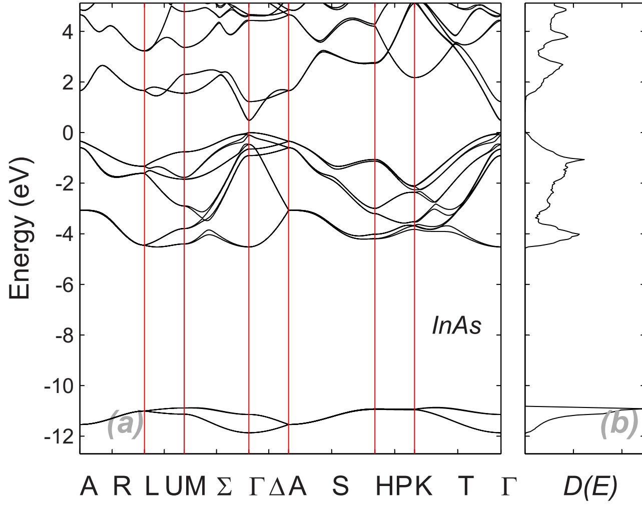

FIG. 11. (Color online) (a) Calculated band structure for InAs in wurtzite phase. (b) Calculated DOS.

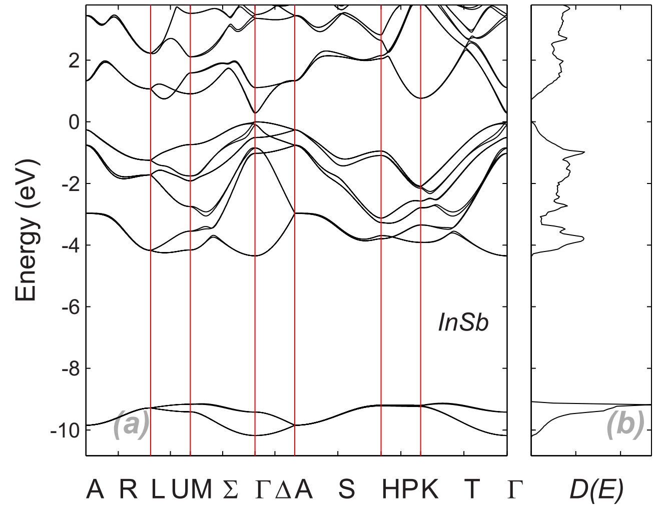

FIG. 12. (Color online) (a) Calculated band structure for InSb in wurtzite phase. (b) Calculated DOS.

value of F was large, indicating a poor fit, the weights W_j were adjusted to climb out of the local minimum in which the algorithm was trapped, and the minimization algorithm was continued.

D. Transferable pseudopotentials

Once the form factors have been determined for the ZB polytype, they may be transferred to the WZ structure by centering the spherically symmetric atomic pseudopotentials on the positions of the ions in the WZ form. The transferability depends on the similarities of the crystal structures, and for sufficiently dissimilar polytypes one would expect the method to fail. Fortunately, as discussed in Sec. II A ZB and WZ are very similar, as the WZ crystal structure can be thought of as a variation of ZB with the same local structure but a slightly different long-range structure. It is important to note that all the parameters were fit independently for each material and the pseudopotentials were transferred between polytypes with the same binary composition. Since the WZ primitive cell has four atoms (rather than the two of ZB), its structure factor contains more terms. Substituting the atomic positions in Sec. II A into Eqs. (7) and (8) the WZ structure factors are

$$S_S = \frac{1}{4}(1 + e^{-iG_3uc})(1 + e^{-iG_2a/\sqrt{3}+G_3c/2}), \qquad (23)$$

TABLE III. Irreducible representaions of zone-center states, energies, effective masses, and linear and cubic Dresselhaus coefficient for the WZ phase of AlP, AlAs, and AlSb. All transition energies are referenced to the top of the valance band for each material.

AlP						AlAs						AlSb					
IR	E (eV)	$m_\parallel$	$m_\perp$	ζ_1 (eV A)	ζ_3 (eV A^3)	IR	E (eV)	$m_\parallel$	$m_\perp$	ζ_1 (eV A)	ζ_3 (eV A^3)	IR	E (eV)	$m_\parallel$	$m_\perp$	ζ_1 (eV A)	ζ_3 (eV A^3)
Γ_7	−12.37	1.351	1.365	0.000	−22.061	Γ_7	−11.763	1.307	1.318	0.000	−28.806	Γ_7	−10.299	1.405	1.424	0.001	−164.203
Γ_8	−10.71	0.550	1.598	0.001	−0.019	Γ_8	−10.131	0.502	1.512	0.113	−0.143	Γ_8	−9.078	0.629	1.820	0.021	−0.186
Γ_8	−6.195	0.298	4.002	0.038	0.115	Γ_8	−6.088	0.280	3.246	0.004	0.256	Γ_8	−5.090	0.319	2.357	0.296	1.485
Γ_8	−1.249	1.655	0.299	0.074	23.745	Γ_8	−1.341	1.608	0.257	0.164	8.293	Γ_8	−1.377	1.611	0.284	0.577	16.066
Γ_9	−1.200	1.662	0.296	0.000	24.557	Γ_9	−1.131	1.658	0.235	0.000	9.896	Γ_9	−0.955	1.667	0.202	0.000	10.236
Γ_7	−0.435	0.145	1.260	0.047	−11.829	Γ_7	−0.518	0.150	0.837	0.140	−59.309	Γ_7	−0.802	0.237	0.971	0.095	−234.420
Γ_7	−0.044	0.931	0.253	0.052	25.634	Γ_7	−0.139	0.478	0.259	0.236	−7.256	Γ_7	−0.156	0.220	0.373	0.125	17.954
Γ_9	0.000	0.972	0.248	0.000	25.032	Γ_9	0.000	0.933	0.216	0.000	10.703	Γ_9	0.000	0.959	0.211	0.000	11.064
Γ_8	2.969	1.187	0.170	0.034	−1.069	Γ_8	1.971	1.081	0.142	0.027	0.635	Γ_8	1.891	1.160	0.157	0.209	−10.332
Γ_7	3.775	0.182	0.157	0.003	−17.969	Γ_7	3.153	0.180	0.141	0.004	76.350	Γ_7	2.418	0.163	0.143	0.005	14.487
Γ_7	4.822	0.924	2.729	0.017	26.128	Γ_7	3.993	0.883	4.253	0.104	6.743	Γ_7	3.384	1.155	1.549	0.054	16.784
Γ_9	4.831	0.923	2.652	0.000	28.017	Γ_9	4.133	0.857	5.281	0.000	31.568	Γ_9	3.577	1.149	3.279	0.000	23.544
Γ_7	5.193	2.263	0.409	0.018	−36.548	Γ_7	4.360	2.806	0.484	0.219	−67.663	Γ_7	3.872	3.705	0.551	0.210	−67.883

TABLE IV. Irreducible representation of zone-center states, energies, effective masses, and linear and cubic Dresselhaus coefficient for the WZ phase of GaP, GaAs, and GaSb. All energies are referenced to the top of the valance band for each material.

GaP						GaAs						GaSb					
IR	E (eV)	$m_{\parallel}$	$m_{\perp}$	ζ_1 (eV Å)	ζ_3 (eV Å^3)	IR	E (eV)	$m_{\parallel}$	$m_{\perp}$	ζ_1 (eV Å)	ζ_3 (eV Å^3)	IR	E (eV)	$m_{\parallel}$	$m_{\perp}$	ζ_1 (eV Å)	ζ_3 (eV Å^3)
Γ_7	−12.942	1.391	1.400	0.000	−10.751	Γ_7	−12.033	1.339	1.350	0.000	−28.285	Γ_7	−10.757	1.270	1.288	0.000	−58.903
Γ_8	−11.369	0.615	1.768	0.076	−0.070	Γ_8	−10.452	0.533	1.520	0.003	−0.089	Γ_8	−9.269	0.452	1.453	0.028	−0.301
Γ_8	−6.313	0.312	2.362	0.064	0.003	Γ_8	−6.289	0.291	12.730	0.188	0.467	Γ_8	−5.992	0.261	3.827	0.344	1.577
Γ_8	−1.327	1.577	0.242	0.105	18.694	Γ_8	−1.291	1.698	0.242	0.440	31.168	Γ_8	−1.537	1.535	0.193	1.137	25.843
Γ_9	−1.233	1.624	0.238	0.000	21.321	Γ_9	−1.049	1.745	0.224	0.000	42.790	Γ_9	−1.030	1.604	0.131	0.000	77.808
Γ_7	−0.373	0.118	1.145	0.068	26.433	Γ_7	−0.475	0.118	0.434	0.048	141.143	Γ_7	−0.874	0.149	0.436	0.147	−141.671
Γ_7	−0.050	0.821	0.210	0.072	35.712	Γ_7	−0.120	0.200	0.197	0.067	67.513	Γ_7	−0.142	0.086	0.192	0.175	23.793
Γ_9	0.000	0.941	0.205	0.000	29.339	Γ_9	0.000	1.026	0.134	0.000	36.419	Γ_9	0.000	0.833	0.087	0.000	73.448
Γ_8	2.251	1.162	0.143	0.075	−3.725	Γ_8	1.503	1.050	0.125	0.212	−12.750	Γ_8	0.509	0.983	0.096	0.716	−72.842
Γ_7	2.877	0.153	0.125	0.006	53.344	Γ_7	1.588	0.090	0.082	0.037	−55.218	Γ_7	0.851	0.064	0.060	0.034	−33.327
Γ_7	4.395	1.135	1.665	0.076	15.714	Γ_7	4.271	0.861	1.977	0.355	62.864	Γ_7	2.824	0.857	1.225	0.184	71.733
Γ_9	4.429	1.233	1.872	0.000	9.533	Γ_9	4.417	0.793	0.722	0.000	123.206	Γ_9	2.970	0.785	0.695	0.000	57.196
Γ_7	4.940	1.510	0.608	0.004	−76.564	Γ_7	4.575	0.974	0.317	0.337	−282.988	Γ_7	3.284	0.394	0.470	0.262	−283.959

$$S_A = \frac{1}{4}(1 - e^{-iG_3uc})(1 + e^{-iG_2a/\sqrt{3}+G_3c/2}), \tag{24}$$

where G_j $(j=1,2,3)$ are the components of the reciprocal lattice vector $\mathbf{G}$.

IV. RESULTS

A. Calculated III-V zinc-blende band structures

The pseudopotential parameters determined by fitting to the zinc-blende band structures are given in Table I including the spin-orbit parameters. The accuracy of the results may be gauged by Table II, which gives the ratio of each band energy to the experimental value to which it was fit.[79] We see that the results agree with experiment to within 1% for all but E_{6v}^{Γ}. Even for E_{6v}^{Γ}, the deviation from the experimental value is greater than 10% only for InSb. We have also made a similar comparison of the effective masses and Luttinger parameters.[79] These values differ from the energy ratios in that the masses were not fit to experimental data. The masses were determined by doing a quadratic fit to the band extremum, with the Luttinger parameters determined from

$$\left(\frac{m^*}{m_{hh(lh)}}\right)^{[001]} = \gamma_1 \mp 2\gamma_2,$$

$$\left(\frac{m^*}{m_{hh(lh)}}\right)^{[111]} = \gamma_1 \pm 2\gamma_3. \tag{25}$$

It should be noted that several of the masses listed in Ref. 79 are either obtained theoretically or have large experimental uncertainties. For example, only theoretically calculated effective masses are available for AlP and for the valence band of AlSb. Experimental results are not available for these compounds. In the case of GaP the conduction-band effective mass is extrapolated from its ternary alloy. For InAs, there is great experimental uncertainty about the heavy and light hole masses.[79] Even though we have omitted nonlocal corrections not associated with spin-orbit coupling, our effective masses are in very good agreement for compounds containing lighter elements.

B. Predicted III-V wurtzite band structures

The calculated band structure and the corresponding DOS for each of the nine III-V semiconductors in WZ phase are shown in Figs. 4–12. The electronic band structures are calculated in the irreducible wedge of the Brillouin zone [Fig. 1(d)]. It should be noted that the band structure of WZ is more complicated than that of ZB due to it lower crystal symmetry and has roughly twice as many bands over a given energy range. The irreducible representations of the zone-center states were determined by transforming the pseudo-wave functions under the symmetry operations of the respective crystallographic point group.

Tables III–V list the calculated zone-center energies of the band extrema, effective masses for $\mathbf{k}$ parallel and perpendicular to the c axis, and the linear and cubic Dresselhaus spin-splitting coefficients ζ_1 and ζ_3. We calculated the Dresselhaus coefficients by fitting a function of the above form in Eq. (2) to the calculated band structures. These parameters may be used in constructing $\mathbf{k}\cdot\mathbf{p}$ WZ Hamiltonians for nanostructure calculations.[42,81–87] We have also complied a summary (Table VI) listing the energy differences most important for nanostructures.

Foremost are the band gap and the irreducible representation of the conduction-band minimum. In our calculations it is seen that all of the materials containing Al or Ga have Γ_8 conduction-band minima in the WZ phase, whereas all of the materials containing In have Γ_7 conduction-band minima. We also give the spin-orbit energy, Δ_{so}, the crystal-field split-

TABLE V. Irreducible representations of zone-center states, energies, effective masses, and linear and cubic Dresselhaus coefficient for the WZ phase of InP, InAs, and InSb. All energies are referenced to the top of the valence band for each material.

InP						InAs						InSb					
IR	E (eV)	$m_{\parallel}$	$m_{\perp}$	ζ_1 (eV A)	ζ_3 (eV A^3)	IR	E (eV)	$m_{\parallel}$	$m_{\perp}$	ζ_1 (eV A)	ζ_3 (eV A^3)	IR	E (eV)	$m_{\parallel}$	$m_{\perp}$	ζ_1 (eV A)	ζ_3 (eV A^3)
Γ_7	−11.746	1.660	1.677	0.000	−28.484	Γ_7	−11.875	2.071	2.034	0.001	−30.395	Γ_7	−10.181	1.802	1.778	0.001	−40.757
Γ_8	−10.711	0.936	2.509	0.036	−0.038	Γ_8	−11.151	1.397	3.377	0.034	−0.116	Γ_8	−9.421	1.094	2.932	0.043	−0.155
Γ_8	−5.091	0.390	1.845	0.087	0.223	Γ_8	−4.526	0.469	1.349	0.088	0.248	Γ_8	−4.351	0.420	1.244	0.004	−0.317
Γ_8	−0.949	1.833	0.237	0.011	3.746	Γ_8	−0.910	2.116	0.210	0.078	5.879	Γ_8	−1.021	2.185	0.222	0.188	2.114
Γ_9	−0.849	1.894	0.230	0.000	2.693	Γ_9	−0.652	2.164	0.166	0.000	27.849	Γ_7	−0.847	0.203	0.210	0.595	633.586
Γ_7	−0.348	0.097	1.205	0.074	97.187	Γ_7	−0.469	0.115	0.319	0.849	744.548	Γ_9	−0.508	2.310	0.206	0.000	7.028
Γ_7	−0.063	0.839	0.169	0.084	65.030	Γ_7	−0.105	0.101	0.113	1.414	648.740	Γ_7	−0.098	0.058	0.094	1.812	178.644
Γ_9	0.000	1.273	0.158	0.000	45.639	Γ_9	0.000	1.700	0.084	0.000	1107.720	Γ_9	0.000	2.060	0.066	0.000	2450.059
Γ_7	1.474	0.105	0.088	0.011	−54.015	Γ_7	0.481	0.060	0.042	0.571	−1143.621	Γ_7	0.287	0.051	0.035	1.212	−2955.560
Γ_8	1.712	1.094	0.132	0.032	−1.600	Γ_8	1.222	1.276	0.113	0.007	−1.456	Γ_8	1.116	1.781	0.118	0.197	−11.492
Γ_7	4.535	1.646	0.952	0.097	70.102	Γ_7	4.445	3.377	0.255	0.790	−106.736	Γ_7	3.395	1.785	2.105	1.909	−44.165
Γ_9	4.575	1.701	0.845	0.000	95.004	Γ_7	4.631	2.025	0.059	0.791	−2927.150	Γ_7	3.513	0.656	1.635	1.987	42.178
Γ_7	4.802	0.804	0.448	0.158	−98.388	Γ_9	4.662	2.580	0.052	0.000	2824.700	Γ_9	3.930	0.565	2.502	0.000	38.729

TABLE VI. Energies of the direct gap III-V WZ semiconductors. The symmetry of the conduction-band minimum is indicated with the band gap. Δ_{so} and Δ_{cr} are the spin-orbit splitting and crystal-field splitting energies extracted using Eq. (26). $\Delta E_{VB} = E_{VB}^{ZB} - E_{VB}^{WZ}$ is the energy difference between the top of the valance bands for the two polytypes.

	E_g (eV)	Δ_{so} (eV)	Δ_{cr} (eV)	ΔE_{VB} (eV)
AlP	2.969 (Γ_8)	0.070	0.409	−0.1428
AlAs	1.971 (Γ_8)	0.319	0.338	−0.0841
AlSb	1.891 (Γ_8)	0.683	0.276	−0.0909
GaP	2.251 (Γ_8)	0.082	0.341	−0.0801
GaAs	1.503 (Γ_8)	0.351	0.244	−0.0632
GaSb	0.509 (Γ_8)	0.777	0.239	−0.1186
InP	1.474 (Γ_7)	0.108	0.303	−0.0646
InAs	0.481 (Γ_7)	0.379	0.195	0.0405
InSb	0.287 (Γ_7)	0.787	0.159	0.0872

ting, Δ_{cr}, and the offset between the valence-band edge of each polytypes. Δ_{so} and Δ_{cr} are extracted using the quasicubic approximation which assumes WZ to be equivalent to [111]-strained ZB,[81,88] with Δ_{so} and Δ_{cr} related to the Γ_{7v} hole energies by

$$E(\Gamma_{7v}^{1,2}) - E(\Gamma_{9v}) = -\frac{\Delta_{so}+\Delta_{cr}}{2} \pm \frac{\sqrt{(\Delta_{so}+\Delta_{cr})^2 - u^{-1}\Delta_{so}\Delta_{cr}}}{2}, \tag{26}$$

where u is related to the lattice constants by $\sqrt{u}=a/c$ and takes the value 3/8 for an ideal WZ structure assumed here.

In the ZB phase, AlP, AlAs, AlSb, and GaP are indirect gap semiconductors with their conduction-band minima ordered X, L, and Γ. Our calculations show that all of the indirect gap ZB semiconductors become direct gap WZ materials with Γ_8 conduction-band minima. Previous LDA calculations obtained indirect gaps for AlP and AlAs in the WZ phase, with the conduction-band minimum at M.[37,38] Although this is not the case in our results, we do find the M valley conduction-band minimum only slightly above the Γ minima (182 meV for AlP and 157 meV for AlAs). The same LDA calculations also predicted AlSb and GaP to have Γ_8 conduction-band minima in agreement with our results.[37] The direct gaps of AlP and AlSb in the WZ phase are larger than the indirect (X-valley) gaps of their respective ZB counterparts; whereas the direct (Γ_8) gaps of AlAs and GaP in WZ phase are smaller than the indirect gaps of their ZB counterparts.

For the direct gap ZB semiconductors GaAs and GaSb, the zone-folded L-valleys result in lower WZ bands gaps with a Γ_8 minimum. For WZ, GaAs has a band gap (≈1.5 eV) which is only slightly smaller than that of its ZB polytype, while GaSb has a significantly smaller gap (≈0.53 eV) in the WZ phase. In both cases this is due to E_{L1c} being close to $E_{\Gamma 1c}$. This behavior is most apparent for GaSb, hence, our prediction for GaSb is consistent with that of Refs. 38 and 37. In light of recent experimental results, the case of WZ GaAs will be discussed in greater detail below. All three indium containing compounds InP, InAs, and InSb are direct gap semiconductors in the WZ phase with Γ_7 conduction-band minima and have higher band gaps than their respective direct gap ZB polytypes.

While little is known about the WZ polytypes, some experimental data are available for the band gaps of GaAs, InAs, and InP. Table VII compares our calculated band gaps for these three materials to experiment and *ab initio* calculations. It should be noted that none of the *ab initio* calculations have included spin-orbit interactions. We have only tabulated the SX and GW results from Ref. 89 as they make different qualitative predictions as to whether the band gap of WZ GaAs is larger or smaller than for ZB. Note that the values listed for the *ab initio* methods are not the direct results from the respective references. The band gaps obtained directly from *ab initio* calculations have well known deficiencies. The *ab initio* band gaps listed in Table VII are instead obtained by comparing the calculated percentage change between the two polytypes and then using the experimental ZB gap to scale the WZ results.

TABLE VII. A comparison between WZ band gaps from empirical pseudopotentials, those obtained from first-principles calculations, and experimental results. The symmetry of the conduction-band minimum is indicated with the band gap. The *ab initio* results are LDA calculations from Refs. 37 and 38, and GW and SX results from Ref. 89. In all three materials our results are in agreement with the experimental values and trends. Note that the *ab initio* values listed are not directly contained in the references, but are obtained from the calculated difference in the band gap between the two polytypes.

	E_g (eV) present calculations	E_g (eV) *ab initio* methods	E_g (eV) experiment
GaAs	1.503 (Γ_8)	1.623[a], 1.6[b], 1.381[c], 1.811[c]	1.498[d], 1.476[e], 1.494[f] 1.51[g]
InP	1.474 (Γ_7)	1.5403[b]	1.44[h] 1.452[i], 1.49[j], 1.508[k], 1.645[l]
InAs	0.481 (Γ_7)	0.6424[b], 0.47[c]	0.54 [l]

[a]Reference 38
[b]Reference 37
[c]Reference 89
[d]Reference 96
[e]Reference 97
[f]Reference 6
[g]Reference 98
[h]Reference 91
[i]Reference 92
[j]Reference 93
[k]Reference 94
[l]Reference 90

As can be seen, our results are in very good agreement with experiments. More importantly, they are in agreement with the experimental trends as to whether the WZ band gap is larger or smaller than the ZB gap. This is most apparent in the case of GaAs, for which *ab initio* calculations (except the SX method[89]) predict that GaAs should have a larger direct band gap in WZ phase than in ZB, in disagreement with experiment. All of the low temperature experimental results show that for GaAs the WZ phase has a smaller band gap than ZB (which suggests that the conduction-band minima for WZ phase GaAs has Γ_8 symmetry instead of Γ_7). In addition, the experimental gaps are obtained from photoluminescence measurements on GaAs nanowires, which will be slightly larger due to confinement. In the case of InP our results are in agreement with experiments as well as with the trends from LDA calculations. In Ref. 90, photocurrent spectroscopy measurements on $InAs_{1-x}P_x$ (for $0.14 < x < 0.48$) nanowires have been extrapolated in x to obtain a band gap for InP of 1.645 eV, which is higher than the values from photoluminescence measurements[91–94] and our calculated results. Similarly, extrapolation to InAs gives a band gap of 0.54 eV,[90] which is also higher than our pseudopotential calculations and may be due to quantum confinement effects in the nanowires.

The spin-orbit coupling can alter the ordering of the valence-band states in different WZ semiconductors. For example, in CdS and CdSe the top three valence states are in descending order Γ_9, Γ_7, Γ_7 (referred to as normal ordering)[59,95] while in ZnO the ordering is Γ_7, Γ_9, Γ_7 (anomalous ordering) which results from a negative spin-orbit energy. In our calculations, all materials except InSb have normal ordering. In the case of InSb the ordering of the valence-band states is complicated by its very large spin-orbit splitting which forces the Γ_7 split-off hole bellow the next Γ_9 state (which comes from the “folded over” *p*-like *L*-valley states in ZB). This results in the unusual Γ_9, Γ_7, Γ_9, Γ_7 ordering of valence-band states in InSb.

Tables III–V also give the Dresselhaus coefficients for each band. As expected,[58] all Γ_9 states have zero linear Dresselhaus coefficients (ζ_1) while all Γ_7 and Γ_8 states have nonzero linear and cubic spin-splitting coefficients. Among the five WZ phase semiconductors with the largest spin-orbit energies (Δ_{so}), InSb has the largest Dresselhaus coefficients, followed by GaSb, InAs, GaAs, and AlSb.

V. SUMMARY

We have calculated the electronic band structure for nine III-V semiconductors in WZ phase using empirical pseudopotentials with the inclusion of spin-orbit coupling. The predicted band structures are based on the concept of transferable model potentials. Our calculations show that in the WZ phase, InP, InAs, and InSb have a direct gap (Γ_7) which is larger than the corresponding zinc-blende material. AlP, AlAs, AlSb, GaP, GaAs, and GaSb also have direct gaps, but with Γ_8 conduction-band minima. WZ AlP and AlAs have larger direct gaps than the indirect gaps of their ZB polytypes. The opposite trend is seen in AlSb and GaP which have smaller direct gaps than their indirect gaps in ZB phase. In the WZ phase GaAs and GaSb have direct gaps which are smaller than their ZB counterparts.

Our calculations are in excellent agreement with experimentally obtained band gaps for GaAs, InAs, and InP in the WZ phase. Significantly, our results agree with experiment over whether the WZ band gap is larger or smaller than the ZB gap in contrast to *ab initio* methods. We have extracted the linear and cubic Dresselhaus spin-splitting coefficients and find they are generally, though not always, larger for materials with larger spin-orbit coupling. The relatively large spin-splittings may be of use for spin-dependent transport in WZ nanowires. More recently, the WZ phase of GaAs has been grown in bulk.[51] More experimental measurements on such bulk WZ phase III–V semiconductors would lead to a clearer understanding of their electronic properties.

ACKNOWLEDGMENT

We would like to acknowledge support from the University of Iowa.

[1] K. Haraguchi, T. Katsuyama, K. Hiruma, and K. Ogawa, Appl. Phys. Lett. **60**, 745 (1992).

[2] K. Hiruma, M. Yazawa, K. Haraguchi, K. Ogawa, T. Katsuyama, M. Koguchi, and H. Kakibayashi, J. Appl. Phys. **74**, 3162 (1993).

[3] B. J. Ohlsson, M. T. Björk, M. H. Magnusson, K. Deppert, L. Samuelson, and L. R. Wallenberg, Appl. Phys. Lett. **79**, 3335 (2001).

[4] H. R. Gutiérrez, M. A. Cotta, and M. M. G. de Carvalho, Appl. Phys. Lett. **79**, 3854 (2001).

[5] P. J. Poole, J. Lefebvre, and J. Fraser, Appl. Phys. Lett. **83**, 2055 (2003).

[6] I. Regolin, V. Khorenko, W. Prost, F. J. Tegude, D. Sudfeld, J. Kästner, G. Dumpich, K. Hitzbleck, and H. Wiggers, J. Appl. Phys. **101**, 054318 (2007).

[7] F. Jabeen, S. Rubini, and F. Martelli, Microelectron. J. **40**, 442 (2009).

[8] C. Colombo, D. Spirkoska, M. Frimmer, G. Abstreiter, and A. Fontcuberta i Morral, Phys. Rev. B **77**, 155326 (2008).

[9] L. Hu and G. Chen, Nano Lett. **7**, 3249 (2007).

[10] L. Tsakalakos, J. Balch, J. Fronheiser, B. A. Korevaar, O. Sulima, and J. Rand, Appl. Phys. Lett. **91**, 233117 (2007).

[11] J. A. Czaban, D. A. Thompson, and R. R. LaPierre, Nano Lett. **9**, 148 (2009).

[12] T. Henry, K. Kim, Z. Ren, C. Yerino, J. Han, and H. X. Tang, Nano Lett. **7**, 3315 (2007).

[13] C. Balocco, A. M. Song, M. Aberg, A. Forchel, T. Gonzalez, J. Mateos, I. Maximov, M. Missous, A. A. Rezazadeh, J. Saijets, L. Samuelson, D. Wallin, K. Williams, L. Worschech, and H. Q. Xu, Nano Lett. **5**, 1423 (2005).

[14] S. Gustavsson, I. Shorubalko, R. Leturcq, T. Ihn, K. Ensslin, and S. Schön, Phys. Rev. B **78**, 035324 (2008).
[15] K. M. Rosfjord, J. K. W. Yang, E. A. Dauler, A. J. Kerman, V. Anant, B. M. Voronov, G. N. Gol'tsman, and K. K. Berggren, Opt. Express **14**, 527 (2006).
[16] C. Zinoni, B. Alloing, L. H. Li, F. Marsili, A. Fiore, L. Lunghi, A. Gerardino, Y. B. Vakhtomin, K. V. Smirnov, and G. N. Gol'tsman, Appl. Phys. Lett. **91**, 031106 (2007).
[17] E. Dauler, B. Robinson, A. Kerman, J. Yang, E. Rosfjord, V. Anant, B. Voronov, G. Gol'tsman, and K. Berggren, IEEE Trans. Appl. Supercond. **17**, 279 (2007).
[18] Y. Cui, Z. Zhong, D. Wang, W. U. Wang, and C. M. Lieber, Nano Lett. **3**, 149 (2003).
[19] A. B. Greytak, L. J. Lauhon, M. S. Gudiksen, and C. M. Lieber, Appl. Phys. Lett. **84**, 4176 (2004).
[20] C. Thelander, T. Mårtensson, M. T. Björk, B. J. Ohlsson, M. W. Larsson, L. R. Wallenberg, and L. Samuelson, Appl. Phys. Lett. **83**, 2052 (2003).
[21] M. T. Björk, B. J. Ohlsson, T. Sass, A. I. Persson, C. Thelander, M. H. Magnusson, K. Deppert, L. R. Wallenberg, and L. Samuelson, Appl. Phys. Lett. **80**, 1058 (2002).
[22] M. T. Björk, B. J. Ohlsson, C. Thelander, A. I. Persson, K. Deppert, L. R. Wallenberg, and L. Samuelson, Appl. Phys. Lett. **81**, 4458 (2002).
[23] N. Panev, A. I. Persson, N. Sköld, and L. Samuelson, Appl. Phys. Lett. **83**, 2238 (2003).
[24] X. Duan, Y. Huang, Y. Cui, J. Wang, and C. M. Lieber, Nature (London) **409**, 66 (2001).
[25] L. Samuelson, C. Thelander, M. T. Bjrk, M. Borgström, K. Deppert, K. A. Dick, A. E. Hansen, T. Mårtensson, N. Panev, A. I. Persson, W. Seifert, N. Sköld, M. W. Larsson, and L. R. Wallenberg, Physica E **25**, 313 (2004); Proceedings of the 13th International Winterschool on New Developments in Solid State Physics–Low-Dimensional Systems (unpublished).
[26] M. Koguchi, H. Kakibayashi, M. Yazawa, K. Hiruma, and T. Katsuyama, Jpn. J. Appl. Phys. **31**, 2061 (1992).
[27] M. Mattila, T. Hakkarainen, M. Mulot, and H. Lipsanen, Nanotechnology **17**, 1580 (2006).
[28] K. Tomioka, J. Motohisa, S. Hara, and T. Fukui, Jpn. J. Appl. Phys., Part 2 **46**, L1102 (2007).
[29] T. Akiyama, K. Nakamura, and T. Ito, Phys. Rev. B **73**, 235308 (2006).
[30] M. Galicka, M. Bukala, R. Buczko, and P. Kacman, J. Phys.: Condens. Matter **20**, 454226 (2008).
[31] F. Glas, J.-C. Harmand, and G. Patriarche, Phys. Rev. Lett. **99**, 146101 (2007).
[32] Y. Haneda, T. Akiyama, K. Nakamura, and T. Ito, Appl. Surf. Sci. **254**, 7746 (2008); 9th International Conference on Atomically Controlled Surfaces, Interfaces and Nanostructures 2007 (ASCIN-9) (unpublished).
[33] V. G. Dubrovskii and N. V. Sibirev, Phys. Rev. B **77**, 035414 (2008).
[34] Q. Xiong, J. Wang, and P. C. Eklund, Nano Lett. **6**, 2736 (2006).
[35] J. Bao, D. C. Bell, F. Capasso, J. B. Wagner, T. Mårtensson, J. Trägårdh, and L. Samuelson, Nano Lett. **8**, 836 (2008).
[36] I. P. Soshnikov, G. Cirlin, A. A. Tonkikh, Y. B. Samsonenko, V. G. Dubovskii, V. M. Ustinov, O. M. Gorbenko, D. Litvinov, and D. Gerthsen, Phys. Solid State **47**, 2213 (2005).
[37] M. Murayama and T. Nakayama, Phys. Rev. B **49**, 4710 (1994).
[38] C.-Y. Yeh, S.-H. Wei, and A. Zunger, Phys. Rev. B **50**, 2715 (1994).
[39] Z. Zanolli, M.-E. Pistol, L. E. Froberg, and L. Samuelson, J. Phys.: Condens. Matter **19**, 295219 (2007).
[40] T. K. Bergstresser and M. L. Cohen, Phys. Rev. **164**, 1069 (1967).
[41] J. D. Joannopoulos and M. L. Cohen, Phys. Rev. B **8**, 2733 (1973).
[42] C. P. Foley and T. L. Tansley, Phys. Rev. B **33**, 1430 (1986).
[43] Z. Z. Bandić and Z. Ikonić, Phys. Rev. B **51**, 9806 (1995).
[44] S. K. Pugh, D. J. Dugdale, S. Brand, and R. A. Abram, J. Appl. Phys. **86**, 3768 (1999).
[45] G. Pennington and N. Goldsman, Phys. Rev. B **64**, 045104 (2001).
[46] D. Fritsch, H. Schmidt, and M. Grundmann, Phys. Rev. B **67**, 235205 (2003).
[47] D. Fritsch, H. Schmidt, and M. Grundmann, Appl. Phys. Lett. **88**, 134104 (2006).
[48] M. Cohen and J. R. Chelikowsky, *Electronic Structure and Optical Properties of Semiconductors* (Springer, Berlin, 1988).
[49] J. L. Birman, Phys. Rev. Lett. **2**, 157 (1959).
[50] I. Vurgaftman and J. R. Meyer, J. Appl. Phys. **94**, 3675 (2003).
[51] M. I. McMahon and R. J. Nelmes, Phys. Rev. Lett. **95**, 215505 (2005).
[52] K. Shimada, T. Sota, and K. Suzuki, J. Appl. Phys. **84**, 4951 (1998).
[53] *Semiconductors Data Handbook*, 3rd ed., edited by O. Madelung (Springer-Verlag, Berlin, 2004).
[54] R. C. Casella, Phys. Rev. **114**, 1514 (1959).
[55] G. F. Koster, J. O. Dimmock, R. G. Wheeler, and H. Statz, *The Properties of the Thirty-Two Point Groups* (MIT Press, Cambridge, MA, 1963).
[56] R. C. Casella, Phys. Rev. Lett. **5**, 371 (1960).
[57] J. J. Hopfield and D. G. Thomas, Phys. Rev. **122**, 35 (1961).
[58] L. C. Lew Yan Voon, M. Willatzen, M. Cardona, and N. E. Christensen, Phys. Rev. B **53**, 10703 (1996).
[59] J. L. Birman, Phys. Rev. **114**, 1490 (1959).
[60] J. J. Hopfield, J. Appl. Phys. **32**, 2277 (1961).
[61] S. L. Adler, Phys. Rev. **126**, 118 (1962).
[62] K. Hümmer, R. Helbig, and M. Baumgärtner, Phys. Status Solidi B **86**, 527 (1978).
[63] I. Broser and M. Rosenzweig, Phys. Status Solidi B **95**, 141 (1979).
[64] E. S. Koteles and G. Winterling, Phys. Rev. Lett. **44**, 948 (1980).
[65] T. Shigenari, X. Z. Lu, and H. Z. Cummins, Phys. Rev. B **30**, 1962 (1984).
[66] D. Culcer, Y. Yao, A. H. MacDonald, and Q. Niu, Phys. Rev. B **72**, 045215 (2005).
[67] W.-T. Wang, C. L. Wu, S. F. Tsay, M. H. Gau, I. Lo, H. F. Kao, D. J. Jang, J.-C. Chiang, M.-E. Lee, Y.-C. Chang, C.-N. Chen, and H. C. Hsueh, Appl. Phys. Lett. **91**, 082110 (2007).
[68] M. Goano, F. Bertazzi, M. Penna, and E. Bellotti, J. Appl. Phys. **102**, 083709 (2007).
[69] J. Y. Fu and M. W. Wu, J. Appl. Phys. **104**, 093712 (2008).
[70] J. C. Phillips and L. Kleinman, Phys. Rev. **116**, 287 (1959).
[71] *Solid State Physics: Advances in Research and Application*, edited by H. Ehrenreich, F. Seitz, and D. Turnbull (Academic Press, London, 1970), Vol. 24.
[72] J.-B. Xia, Phys. Rev. B **38**, 8358 (1988).
[73] C.-Y. Yeh, S. B. Zhang, and A. Zunger, Phys. Rev. B **50**, 14405 (1994).

[74] W. J. Fan, J. B. Xia, P. A. Agus, S. T. Tan, S. F. Yu, and X. W. Sun, J. Appl. Phys. **99**, 013702 (2006).
[75] G. Weisz, Phys. Rev. **149**, 504 (1966).
[76] L. R. Saravia and D. Brust, Phys. Rev. **176**, 915 (1968).
[77] J. R. Chelikowsky and M. L. Cohen, Phys. Rev. B **14**, 556 (1976).
[78] F. Herman and S. Skillman, *Atomic Structure Calculations* (Prentice-Hall, Englewood Cliffs, NJ, 1963).
[79] I. Vurgaftman, J. R. Meyer, and L. R. Ram-Mohan, J. Appl. Phys. **89**, 5815 (2001).
[80] M. L. Cohen and T. K. Bergstresser, Phys. Rev. **141**, 789 (1966).
[81] S. L. Chuang and C. S. Chang, Phys. Rev. B **54**, 2491 (1996).
[82] Y. C. Yeo, T. C. Chong, and M. F. Li, J. Appl. Phys. **83**, 1429 (1998).
[83] A. A. Sirenko, T. Ruf, M. Cardona, D. R. Yakovlev, W. Ossau, A. Waag, and G. Landwehr, Phys. Rev. B **56**, 2114 (1997).
[84] J.-B. Xia and J. Li, Phys. Rev. B **60**, 11540 (1999).
[85] F. Mireles and S. E. Ulloa, Phys. Rev. B **62**, 2562 (2000).
[86] A. V. Rodina and B. K. Meyer, Phys. Rev. B **64**, 245209 (2001).
[87] R. Beresford, J. Appl. Phys. **95**, 6216 (2004).
[88] G. L. Bir and G. E. Pikus, *Symmetry and Strain-Induced Effects in Semiconductors* (Halsted, Jerusalem, 1974).
[89] Z. Zanolli, F. Fuchs, J. Furthmuller, U. von Barth, and F. Bechstedt, Phys. Rev. B **75**, 245121 (2007).
[90] J. Trägårdh, A. I. Persson, J. B. Wagner, D. Hessman, and L. Samuelson, J. Appl. Phys. **101**, 123701 (2007).
[91] M. Mattila, T. Hakkarainen, H. Lipsanen, H. Jiang, and E. I. Kauppinen, Appl. Phys. Lett. **90**, 033101 (2007).
[92] S. Reitzenstein, S. Münch, C. Hofmann, A. Forchel, S. Crankshaw, L. C. Chuang, M. Moewe, and C. Chang-Hasnain, Appl. Phys. Lett. **91**, 091103 (2007).
[93] A. Mishra, L. V. Titova, T. B. Hoang, H. E. Jackson, L. M. Smith, J. M. Yarrison-Rice, Y. Kim, H. J. Joyce, Q. Gao, H. H. Tan, and C. Jagadish, Appl. Phys. Lett. **91**, 263104 (2007).
[94] Y. Ding, J. Motohisa, B. Hua, S. Hara, and T. Fukui, Nano Lett. **7**, 3598 (2007).
[95] D. G. Thomas and J. J. Hopfield, Phys. Rev. **116**, 573 (1959).
[96] K. Haraguchi, T. Katsuyama, and K. Hiruma, J. Appl. Phys. **75**, 4220 (1994).
[97] I. Soshnikov, G. Cirlin, V. Dubrovskii, A. Veretekha, A. Gladyshev, and V. Ustinov, Phys. Solid State **48**, 786 (2006).
[98] V. Khorenko, I. Regolin, S. Neumann, W. Prost, F.-J. Tegude, and H. Wiggers, Appl. Phys. Lett. **85**, 6407 (2004).